Catalysis Today xxx (xxxx) xxx–xxx

Contents lists available at ScienceDirect

Catalysis Today

journal homepage: www.elsevier.com/locate/cattod

Hydrodeoxygenation of guaiacol using NiMo and CoMo catalysts supported on alumina modified with potassium

Iván D. Mora-Vergara[a], Linney Hernández Moscoso[a], Eric M. Gaigneaux[b], Sonia A. Giraldo[a], Víctor G. Baldovino-Medrano[a,*]

[a] Centro de Investigaciones en Catálisis (@CICATUIS), Escuela de Ing. Química, Universidad Industrial de Santander (UIS), Parque Tecnológico de Guatiguará, Km 2 vía El Refugio, Piedecuesta, Santander, 681011, Colombia

[b] Institute of Condensed Matter and Nanosciences – IMCN, Division « Molecules, Solids and Reactivity–MOST », Université Catholique de Louvain, Croix du Sud 2 L7.05. 15, B-1348 Louvain-la-Neuve, Belgium

ARTICLE INFO

Keywords:
Hydrodeoxygenation
Guaiacol
CoMo
NiMo
Alumina
Potassium

ABSTRACT

Bio-oils require the elimination of most of the oxygen they contain to stabilize them before their use as fuels. The hydrodeoxygenation (HDO) process consists on eliminating oxygen from the bio-oil at high hydrogen pressures over a solid catalyst. However, catalysts often suffer from prompt deactivation due to extensive coke deposition. Therefore, searching more stable catalysts for HDO is still a challenge for biorefiners. In this work, the HDO of guaiacol as a model compound from bio-oil was carried out in a batch reactor at 523 K, p_{H2} = 5.5 MPa over potassium modified γ-Al_2O_3 supported CoMo and NiMo catalysts. Potassium was shown to be an effective activity and selectivity modifier. It led to an increase in the yields to products that may hinder catalysts coking by shifting selectivity from demethylation and methyl substitution reactions to direct $\boldsymbol{C_{Aromatic}-OH}$ bond scission and hydrogenation reactions. Changes on selectivity were accompanied by a decrease in guaiacol conversion. The effect produced by potassium was shown to be related to: a reduction in acidity, a decrease in the relative number of Mo species in octahedral coordination, and to an increase in the relative concentration of catalytically inactive $NiAl_2O_4$ and $CoAl_2O_4$ species. Results of this work contribute to design more stable HDO catalysts from a rather simple modification of conventional hydrotreatment catalysts.

1. Introduction

The high consumption of fossil fuels, the environmental impact generated by their use, and the reduction of their reserves continue to spark interest in finding new cleaner energy sources. Among the available options to do so, the processing of residual biomass by fast pyrolysis which leads to bio-oils is the most important one. Pyrolysis bio-oils can be exploited as an energy source due to their similarity to petroleum fuels and to their low content of molecules containing sulfur and nitrogen [1,2]. However, they contain a significant amount of water (15–40 wt%) as well as plenty of organic oxygenates compounds (10–40 wt%). The latter make them highly viscous, highly acidic, thermally instable and of low calorific value [3].

The catalytic hydrodeoxygenation (HDO) of pyrolysis bio-oils transforms them to suitable transportation fuels [4]. Although, the HDO of pyrolysis bio-oils cannot normally be performed in a single stage process, as it is the case for conventional HDO, due to enormous variations in the reactivity of the molecules that constitutes the bio-oil feed [4,5]. In a typical two stage HDO process, the first stage consists of a stabilization of the bio-oil at low temperature (473–553 K). During this stage, the most reactive functional groups of the organic molecules such as those in ketones, esters, carboxylic acid, aldehyde and those from the methoxy linkage ($\boldsymbol{C_{Aromatic}-O-CH_3}$) of guaiacol; i.e. 2-methoxyphenol, are converted or broken to yield molecules provided of more stable phenolic ($\boldsymbol{C_{Aromatic}-OH}$) type bonds. The second stage, which takes place at a temperature above 553 K, carries out the hydrodeoxygenation of the phenolic bonds as well as the more refractory methoxy group of furanes. It is only after this stage that a fuel similar to those from petroleum is obtained.

Guaiacol is often used as a model molecule in HDO studies. The methoxy and hydroxy functional groups of the molecule are responsible for its low thermal stability and high tendency to form high molecular weight compounds during the process. Furthermore, the HDO of guaiacol over conventional catalytic materials is known to produce large amounts of surface coke over the employed catalysts [6].

A first HDO stage for guaiacol over conventional hydrodesulfurization

* Corresponding author.
E-mail addresses: vicbaldo@uis.edu.co, vicbaldo@saber.uis.edu.co (V.G. Baldovino-Medrano).

http://dx.doi.org/10.1016/j.cattod.2017.07.015
Received 21 December 2016; Received in revised form 26 June 2017; Accepted 8 July 2017

(HDS) catalysts; i.e. alumina supported sulfided CoMo and NiMo, leads to fully deoxygenated products such as toluene, benzene, and cyclohexane, and to phenol as a partially deoxygenated compound. However, highly undesirable reactions such as the methyl substitution of the aromatic ring and the formation of high molecular weight compounds are also present [7,8]; both of which are known coke precursors that rapidly deactivate the catalysts.

Centeno et al. [9], Sepúlveda et al. [10], and Nimmanwudipong et al. [11]; employing sulfided CoMo/$\gamma - Al_2O_3$, Re/$\gamma - Al_2O_3$ and Pt/$\gamma - Al_2O_3$ catalysts, respectively, reported the formation of methylated compounds over them. They attributed this effect to the acidity of the support. Therefore, a way to inhibit this type of reactions is modifying the acid-base properties of the alumina support. Busca [12] proposed the use of alkali ions as dopants of transition metal oxides and metal catalysts to reduce their acidity. Montanari et al. [13] by FTIR and NO_2 TPD found that loading alumina with 1–5 wt.% potassium led to a loss of Brønsted and Lewis acidity from surface hydroxyls and Al^{+3} vacancies, respectively. Likewise, Pérez et al. [14] found similar results and used potassium loaded aluminas as supports for CoMo catalysts for the hytrotreatment of FCC naphtha. Authors showed that potassium is an effective modulator of the catalytic performance in this kind of reactions.

In this work, the effects of loading potassium on the alumina support of CoMo and NiMo catalysts aimed for the HDO of guaiacol were investigated. The surface properties of the oxide precursors of the sulfided catalysts were analyzed in terms of their porosity (N_2 physisorption tests), acidic properties (Proton Affinity Distribution −PAD– analyses), composition and electronic state of the metals (X-ray photoelectron spectroscopy −XPS– measurements), and molecular structure (UV–vis Difusse Reflectance Spectroscopy −UV–vis DRS– analyses). A correlation between the changes induced by potassium on the acidity and molecular structure of the metallic oxide precursors of the catalysts was found.

2. Experimental

2.1. Catalysts preparation

CoMo and NiMo materials containing 10 wt.% MoO_3 and 3 wt.% CoO or NiO supported on 1 and 3 wt.% potassium loaded γ-Al_2O_3 (*Procatalyse*) were prepared by the successive incipient wetness impregnation method. Aqueous solutions of appropriate concentrations of $(NH_4)_6Mo_7O_{24}{\cdot}4H_2O$ (Merck, 99%), $Co(NO_3)_2{\cdot}6H_2O$ (Sigma Aldrich 99.5%), $Ni(NO_3)_2{\cdot}6H_2O$ (Carlo Erba 99%), and KNO_3 (Merck, 99%) were used for impregnation. After each impregnation step, solids were dried under air flow (100 cm^3/min) at 393 K for 12 h and finally air calcined at 773 K for 4 h. Catalysts modified with potassium were named CoMo/A-K(x) and NiMo/A-K(x). Where, x represents the nominal content of potassium and A stands for the $\gamma - Al_2O_3$ support. CoMo/$\gamma - Al_2O_3$ and NiMo/$\gamma - Al_2O_3$ catalysts were prepared as references and named CoMo/A and NiMo/A, respectively.

2.2. Catalysts characterization

2.2.1. Textural properties

The specific BET surface area (SA_{BET}), pore volume (PV) and average pore diameter (PD) of the materials were estimated by means of nitrogen adsorption-desorption isotherms at 77 K using a 3Flex apparatus from Micromeritics. SA_{BET} was calculated using the C_{BET} optimization procedure suggested by Rouquerol et al. [15]. The PV and the PD were calculated from the method of Barrett, Joyner and Halenda (BJH) [16]. Calculations were performed with the adsorption branch of the isotherms as in agreement with IUPAC recommendations [17]. The data analysis software provided with the instrument was employed. This software assumes a cylindrical pore shape for BJH. Prior to the measurements, samples of ca. 0.2 g of each material were outgassed under vacuum at 393 K for ca. 12 h. At these conditions, a final pressure of 0.05 mbar was always reached.

A normalized specific surface area (NSA_{BET}) was calculated applying the method presented in [18] and in order to assess pore blocking effects:

$$NSA_{BET} = \frac{SA_{BET}\ of\ the\ oxide\ catalyst\ precursors}{SA_{BET}\ of\ the\ supports^{*}(1-y)} \quad (1)$$

Where, "y" is the weight fraction of the metallic phases.

Values of NS_{BET} near 1 suggest that the metallic phases are well dispersed on the support hence not causing an obstruction of its pores. The contrary is suggested when NS_{BET} is far below 1. This formula has been used in a previous work with satisfactory results [19].

2.2.2. X-Ray photoelectron spectroscopy

The surface chemical state of the materials was studied by XPS. Measurements were carried out in an SSI-X-probe spectrometer (SSX-100/206, Surface Science Instruments) equipped with a monochromatic microfocused Al Kα (1486.6 eV) X-ray source (10 kV; 22 mA). Particles of the oxide precursors of the catalysts were pressed into small stainless steel troughs mounted on a multi-specimen ceramic sample holder. The analysis chamber was operated under ultrahigh vacuum with a pressure close to 5×10^{-7} Pa. Charge stabilization was achieved by using an electron flood gun adjusted at 8 eV and placing a nickel grid 3 mm above the samples. The following sequence of spectra was recorded: general spectrum, C 1s + K 1s, O 1s, Co 2p, Ni 2p, Mo 3d, and C 1s again to check the stability of charge compensation as a function of time. All but the general spectra were recorded fixing the pass energy at 50 eV. The analyzed area was approximately 1.4 mm^2. The spectra were decomposed with the CasaXPS program (Casa Software Ltd.) employing a Gaussian/Lorentzian (85/15) product function after subtraction of a Shirley nonlinear sigmoid-type baseline. The binding energy (BE) scale was corrected by using the C-[C, H] component of the adventitious carbon peak at 284.8 eV as a reference.

2.2.3. Proton affinity distributions

The acid-base properties of the supports and oxide precursors of the sulfided catalysts were determined by potentiometric titration using a TitroLine Alpha (Schott, ± 0.001 pH units) instrument. Samples of 0.5 g of the oxide precursors of the catalysts, particle size (Dp) < 75 µm, were suspended in 50 cm^3 of an aqueous solution of $NaNO_3$ 0.1 M kept at constant magnetic stirring to stabilize pH. Aqueous solutions of HNO_3 0.1 N and NaOH 0.1 N were used as acid and basic titrants, respectively. These solutions were added in a volume of 0.05 cm^3 every 90 s until reaching a final pH of 3 or 11. Each one of these measurements was performed with fresh samples. pH values recorded as a function of the accumulated volumes of acid or base titrants were employed for constructing proton consumption (F(LogK)) curves via a proton balance [20–22]. The quantification of the surface OH groups of the supports was carried out by decomposing PAD curves with Gaussian functions as in agreement with the method reported by Contescu et al. [22] and employing the software *OriginPro 8.5.1*. For the analyses, the area under the curve of each peak was assumed to represent the number of acid sites (mmol H^+/g·cat).

2.2.4. UV–vis difusse reflectance spectroscopy

The chemical structure of the oxides of cobalt, nickel and molybdenum in the catalysts oxide precursors was determined from UV–vis DRS spectra. A UV-2401PC Shimadzu spectrophotometer equipped with an ISR 240A integrating sphere accessory was used. Spectra were recorded in the range 200–800 nm and using $BaSO_4$ as a reference. The Kubelka-Munk function was calculated from reflectance by F(R), where R is the diffuse reflectance depending on the wavelength.

2.3. Catalysts evaluation

The performance of the catalysts was tested in the HDO of guaiacol. Catalytic tests were carried out in a stainless-steel *batch* reactor (Parr instruments) at 523 K, under a H_2 pressure of 5.5 MPa and a stirring rate of 750 rpm. 1.7 g of catalyst (Dp: 0.3–0.6 mm) were employed for each test. A solution of 250 cm^3 of reactants was prepared using 3.7 wt. % of guaiacol (Sigma-Aldrich, 98%), xylenes containing ethylbenzene (J.T. Baker, 99.9%) as solvent, and 2 wt.% dodecane (Sigma-Aldrich, 99%) as an internal standard for gas chromatography (GC) quantification. The oxide precursors of the catalysts were sulfided *ex-situ* under an H_2S/H_2 (15/85% v/v) flow of 100 cm^3/min at 673 K for 4 h. A catalyst-to-guaiacol ratio of 0.21 was fixed for the reaction tests. The reactor was sealed immediately after adding the catalyst to the reaction feed. Remnant air was evacuated by performing pressurization-depressurization cycles with nitrogen. The reaction mixture was then heated to 523 K at a constant stirring of 750 rpm. Once the reaction temperature was reached, the system was pressurized to 5.5 MPa with H_2. After reaching reaction conditions, the first liquid sample of reaction products was taken and considered as zero reaction time. Constant pressure was maintained for the entire duration of the catalytic tests by adding H_2 to the reactor whenever necessary. Liquid samples were periodically withdrawn during the course of the reaction after purging the sampling line with the reaction feed. Samples were taken every 10 min during the first hour of reaction, every 20 min during the second hour, and every 30 min during the third and fourth hours of time on stream. The volumes from the liquid products and from the purge withdrawn from the reactor were systematically measured. Liquid samples were analyzed by Gas Chromatography with a HP 6890 instrument equipped with a HP-1 column (100 m × 0.25 mm × 0.5 μm) and an FID detector. The split-splitless inlet was operated at 473 K, 2.4 bar, and 85.914 cm^3/min of He. The oven of the instrument was programmed with a temperature ramp consisting on holding temperature at 363 K then raising it to 403 K. This temperature was held for 8.5 min. Afterwards, temperature was raised to 453 K and held under this condition for 0.5 min. Finally, temperature was raised to 493 K and held at this condition for 3.0 min. A temperature rate of 5 K/min was always used for the analyses. Unidentified reaction products were further analyzed by GC–Mass spectrometry using an HP-5 MS column. The carbon mass balance was verified for all reaction tests.

2.4. Expression of the catalytic results

The reaction kinetics of HDO was assessed considering a pseudo first reaction order with respect to guaiacol [8,23]. The catalytic activity was expressed by means of the initial reaction rate constant (k) as calculated by a lineal regression of Eq. (2) and introducing a volume correction factor as according to Eq. (3). This method is in agreement with that proposed by Gevert et al. [24]:

$$-\ln\left(C_i/C_0\right) = k_{GUA} W f\left(t/V\right) \tag{2}$$

$$f\left(t/V\right) = \sum_{i=1}^{n} \frac{t_i - t_{i-1}}{V_{i-1}} \tag{3}$$

Where, C_i and C_0 [g/cm^3] are guaiacol concentrations for sample i at time t and at time zero; k [cm^3/min g] is the reaction rate constant; W [g] is the catalyst weight; V [cm^3] is the reaction volume; t [min] is the reaction time and n is the number of samples taken during the catalytic tests.

The apparent reaction rate was calculated from expression (4):

$$r_{gua} = k_{GUA} * C_{gua} \tag{4}$$

Where, r_i [mol/min g] is the apparent reaction rate, and C_{gua} is guaiacol concentration.

A specific reaction rate r_i [molec./min Mo at.] can be calculated from Eq. (5):

$$r_i = r/n * N \tag{5}$$

Where, n is the number of Mo atoms per g of catalyst and N is the Avogadro number.

Products yields were calculated using Eq. (6):

$$yield = mol_j / mol_0^{gua} \tag{6}$$

Where, mol_j are the moles of product j and mol_0^{gua} are the initial moles of guaiacol. Further details on these calculations are presented in the Supplementary Information.

Table 1
Surface area (SA_{BET}), pore volume (PV), C_{BET} constant, and normalized specific surface area (NSA_{BET}) for the supports and oxide catalysts precursors.

Catalyst	SA_{BET} (m^2/g)	PV (cm^3/g)	C_{BET}	NSA_{BET}
A	224	0.61	114	1.00
A-K(1)	211	0.60	129	0.96
A-K(3)	198	0.58	154	0.91
CoMo/A	174	0.45	173	0.89
CoMo/A-K(1)	176	0.49	175	0.91
CoMo/A-K(3)	172	0.50	144	0.91
NiMo/A	178	0.47	173	0.91
NiMo/A-K(1)	174	0.49	181	0.90
NiMo/A-K(3)	159	0.46	138	0.85

3. Results and discussion

3.1. Influence of potassium on the textural properties of the catalysts

The textural properties of the supports and oxide precursors of the catalysts as well as the values of NSA_{BET} are presented in Table 1. The incorporation of the active metals onto the support diminished to some extent the SA_{BET} as well as the pore volume of the materials. On the other hand, according to NSA_{BET} values, no extensive pore blocking occurred after the incorporation of the potassium, cobalt, nickel, and molybdenum oxides onto the alumina [25]. BJH pore size distributions did not exhibit a detectable change in the supports with the incorporation of potassium (Supplementary information: Fig. S1). Conversely, plots for BJH pore size distributions for NiMo/A-K(x) (Fig. 1) and CoMo-K(x) (Supplementary information: Fig. S2) evidence pore narrowing as in agreement with the decrease in NSA_{BET}. It is important to remark that this pore narrowing is coherent with a good dispersion of the metals over the alumina. The average pore diameter of the supports and catalysts was around 13 nm (Fig. 1 and Figs. S1 and S2).

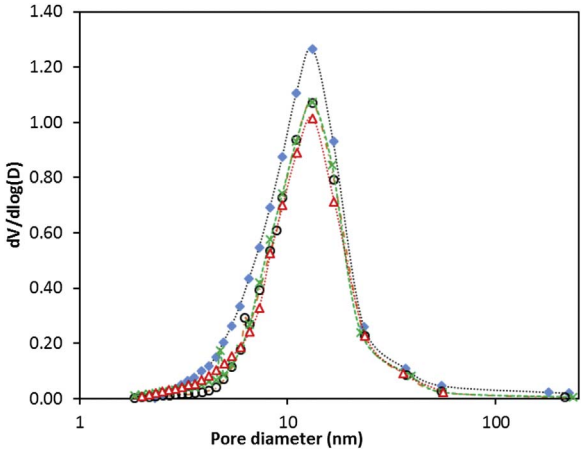

Fig. 1. BJH pore size distributions for alumina (-♦-), NiMo (-**O**-), NiMo-K(1) (--X--) and NiMo-K(3) (··Δ··).

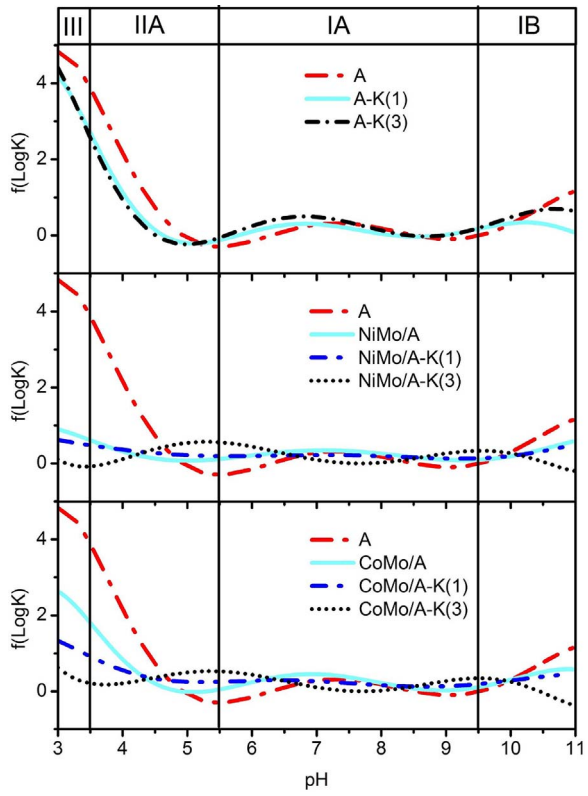

Fig. 2. PAD curves for the supports (a), NiMo/A-K(x) catalysts (b), and CoMo/A-K(x) catalysts (c).

3.1.1. Influence of potassium on the acid-base properties of the materials

PAD curves for alumina and potassium modified alumina are presented in Fig. 2. In general, curves exhibited three well-defined peaks at pHs near to 3.7 and 11. These peaks were decomposed and quantified into four contributions (Table 2) corresponding to the hydroxyl groups identified by Contescu et al. [20]. Namely, OH groups of the types III, IIA, IA and IB. The original works of Knözinger [26] presented such a classification: OH groups of the type III are the most acidic, type IIA have an intermediate character and type IA and IB are the most basic. Besides, the OH groups of the different types are coordinated with Al^{+3} cations: in octahetral coordination to type III, in tetrahedral and octahedral coordination to type IA and IB, and in octahedral and tetrahedral coordination to type IIA.

From Table 2, results of the decrease percentage in the relative concentration of alumina hydroxyls due to potassium show that type III sites prevail on the surface of alumina followed by type IIA sites. According to calculations, potassium mostly occupies IIA sites but also diminished the relative concentration of all of its hydroxyls. Therefore, potassium diminished the total acidity of alumina. These results agree with those reported by De Miguel et al. [27] who used IR analyses of adsorbed CO to study the adsorption of potassium over alumina. Authors proposed the formation of a basic $[\equiv Al{-}OH]^{-}K^{+}$ surface complex [28,29] to explain the decrease in acidity. For alumina, it is remarkable that IA hydroxyls increased for a potassium loading of 3 wt. %. This may be explained considering that under such conditions the surface hydroxyl groups associated to the $[\equiv Al{-}OH]^{-}K^{+}$ increase in concentration and overlap with the original IA hydroxyls from the alumina. Such a hypothesis seems reasonable since the basic nature of both types of sites is similar.

In general, PAD curves of the oxide precursors of the catalysts without modifying were very similar (Figs. 2b and c) and it was found that all OH groups decreased after the incorporation of the metallic phases (Table 2). However, the decrease was more significant in type IIA sites, which indicates that metals could have some preference to attach on these sites. This is in agreement with an IR spectroscopic study of the OH groups in calcined CoMo over alumina which revealed that type IIA sites are selectively eliminated through reaction with Mo [30]. A general comparison of the PAD results indicates that potassium mostly consumes IIA type hydroxyls which are also the preferred sites for the metallic NiMo and CoMo oxide species. Henceforward, when these metals are impregnated onto the potassium modified support they tend to occupy the other surface hydroxyls of the support without seemingly having a particular preference.

Regarding PAD curves for CoMo/A-K (3) and NiMo/A-K(3), showed in Figs. 2b and c respectively, the disappearance of the peak corresponding to type IA OH sites and the appearance of peaks at pHs 5.5 and 9.5 were observed. This phenomenon may be associated to the emergence of new sites with weaker acid characteristics as it was suggested by Contescu et al. [20].

3.1.2. Influence of potassium on the chemical structure of the materials

Figs. 3a and b show the UV–vis DRS spectra in the wavelength region between 200 and 400 nm for samples of CoMo/A-K(*x*) and NiMo/A-K(*x*), respectively. Unmodified materials CoMo/A and NiMo/A exhibited four distinguishable bands at ca. 223, 243, 274, and 309 nm. The modification of alumina with potassium led to the disappearance of these bands. Except for the band around 225 nm, a significant decrease in the intensity of the entire spectra ascribed to $Mo^{(VI+)}$ species was observed. In literature, the distinction between octahedral and tetrahedral Mo species via UV–vis DRS characterization has been investigated extensively. Authors such as Mendoza et al. [31] ascribed tetrahedral species to bands around 250 nm and octahedral species to bands between 260 and 330 nm. On the other hand, Jeziorowski and Knözinger [32] assigned bands around 230–240 nm to isolated tetrahedrally coordinated Mo centers and bands ranging from 250 to 290 nm to bridging Mo-O-Mo structures species. Furthermore, Plyuto et al. [33] attributed the region between 280 and 295 nm to molybdenum from octahedral species. Therefore, Mo species in tetrahedral coordination are usually ascribed to UV–vis DRS bands in the region between 220 and 250 and the octahedral coordination in the region between 250 and

Table 2
Quantification of types of OH groups for the supports and the oxidic precursors of the catalysts.

Catalyst	Quantification of the detected hydroxyls by type [mmol H^{+}/g catalyst]				% Decrease with respect to alumina			
	III	IIA	IA	IB	III	IIA	IA	IB
A	2.596	1.250	0.602	0.727	21.1	60.6	22.4	32.2
A-K(1)	2.049	0.492	0.467	0.493	16.1	68.9	***−12.6***	4.8
A-K(3)	2.178	0.389	0.678	0.692	84.0	97.8	56.3	64.8
NiMo/A	0.415	0.028	0.263	0.256	90.6	90.9	86.7	74.8
NiMo/A-K(1)	0.243	0.114	0.080	0.183	44.9	88.7	21.8	48.6
CoMo/A	1.431	0.141	0.471	0.374	77.6	85.0	74.1	73.6
CoMo/A-K(1)	0.581	0.187	0.156	0.192	21.1	60.6	22.4	32.2

The bold value means an increase, in comparison with unmodified alumina, of the concentration of OH groups similar to type IA

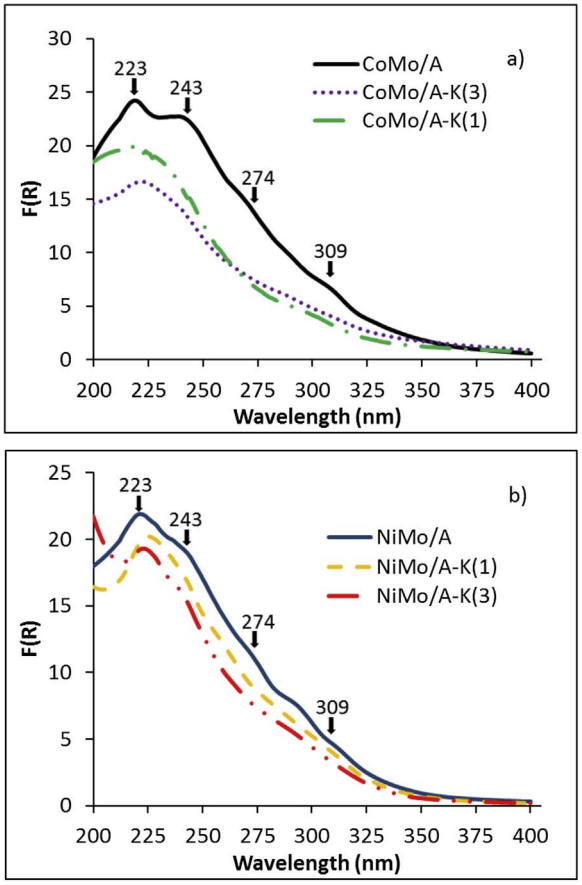

Fig. 3. UV–vis DRS spectra recorded in the range 200–400 nm for: (a) CoMo/A-K(x); (b) NiMo/A-K(x).

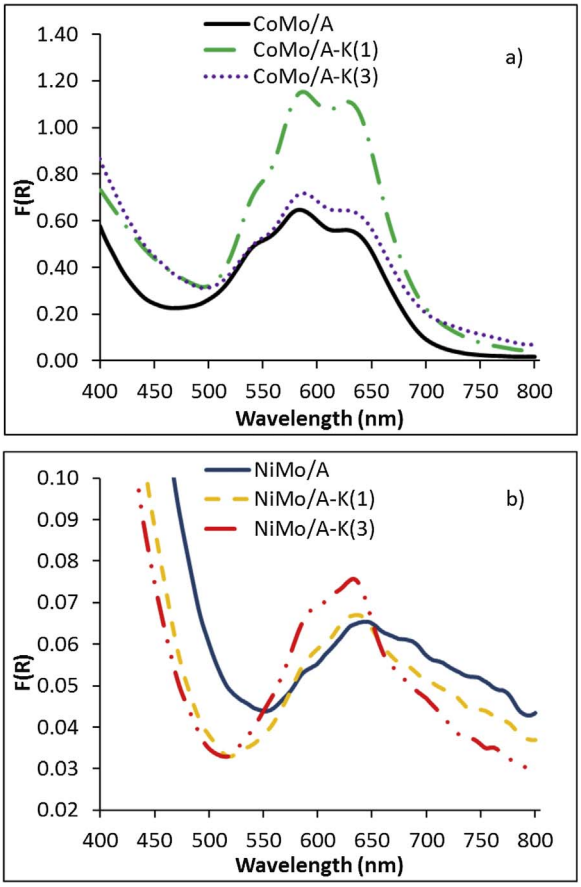

Fig. 4. UV–vis DRS spectra recorded in the range 400–800 nm for: (a) CoMo/A-K(x) catalysts; (b) NiMo/A-K(x) catalysts.

330 nm. Per such a conclusion, results presented herein indicate that potassium promotes a decrease in the relative concentration of Mo octahedral since a decrease in the intensity of the bands around 243, 274 and 309 was recorded whereas the intensity of the band around 225 nm remained rather constant. Considering such trends, it might be expected that potassium modifies the molecular structure of the Mo oxide species which are precursors of the sulfided active phase catalysts [14,34].

UV-vis DRS spectra for CoMo/A-K(x) and NiMo/A-K(*x*) in the region 400–800 nm are presented in Figs. 4a and b, respectively. For CoMo/A-K(*x*) (Fig. 4a), the triple band centered at about 600 nm is attributed to Co^{2+} species in tetrahedral coordination such as those typically ascribed to a $CoAl_2O_4$ spinel [35,36]. Additionally, the spectra showed evidence of the formation of Co_3O_4. Particularly, since the bands at 450 and 750 nm are attributed to Co^{2+} species in tetrahedral coordination or Co^{3+} in octahedral coordination [35,36]. Fig. 4a shows that the intensity of the triple band at 450 and 750 nm increased with the incorporation of potassium. This may suggest that potassium promotes the formation of $CoAl_2O_4$ and Co_3O_4 phases in CoMo/A-K(*x*). The presence of $CoAl_2O_4$ species in the CoMo/A oxide precursors of the sulfided catalysts has negative effects for the hydrotreatment reactions because Co atoms in the $CoAl_2O_4$ spinel are difficult to sulfide hence not contributing to the activity of the corresponding sulfide catalysts [36]. For the Ni species, Fig. 4b, the addition of potassium to the NiMo/A system led to an increase in the intensity of the absorption bands between 590 and 640 nm. Ni species observed within such wavelengths are associated to Ni^{2+} species in tetrahedral coordination such as those forming a $NiAl_2O_4$ spinel phase [37–39]. This result is similar to the one previously presented for CoMo/A. Additionally, the modification with potassium decreased the intensity of the spectra in the region between 680 and 760 nm (Fig. 4b). According to literature, this region is associated to Ni^{2+} species octahedrally coordinated to MoO_4^{2-} ions [40]. Such species are considered precursors of the sulfide active phase of these catalysts. In conclusion, the evidence collected by DRS indicated that the addition to potassium promotes the formation of $CoAl_2O_4$ and $NiAl_2O_4$ spinels while for Ni promoted materials, potassium also hampers the formation octahedrally coordinated Ni^{2+} species. Consequently, a relatively lower concentration of the active sulfided species of the catalysts might be expected [36,41].

3.1.3. XPS characterization

Table 3 presents the normalized XPS quantification (mole%) for the prepared materials. Original .vms files suitable for data treatment in CasaXPS are appended as Supplementary Information. Firstly, the mole percentage of surface potassium on alumina; samples A, A-K(1), and A-

Table 3
XPS surface elemental quantification.

[a]Catalyst	Normalized XPS quantification (mole%)					
	O	K	Al	Mo	Co	Ni
A	65.22	0.00	34.78	–	–	–
A-K(1)	62.64	1.74	35.62	–	–	–
A-K(3)	64.63	5.66	29.72	–	–	–
CoMo/A	65.17	0.00	32.13	1.70	1.00	–
CoMo/A-K(1)	64.73	1.37	31.50	1.53	0.87	–
CoMo/A-K(3)	60.34	6.52	27.82	2.93	2.39	–
NiMo/A	64.53	0.00	32.92	1.77	–	0.77
NiMo/A-K(1)	62.78	1.16	33.80	1.57	–	0.68
NiMo/A-K(3)	64.49	4.02	29.38	1.26	–	0.85

[a] A = Al_2O_3, numbers in parentheses are potassium loadings in wt%.

Table 4
Active metals surface mole ratios as measured by XPS.

Catalyst	Active metals surface mole ratios		
	Mo/(Al + O + K)	Co/(Al + O + K)	Ni/(Al + O + K)
CoMo/A	0.017	0.010	0.000
CoMo/A-K(1)	0.016	0.009	0.000
CoMo/A-K(3)	0.032	0.026	0.000
NiMo/A	0.018	0.000	0.008
NiMo/A-K(1)	0.016	0.000	0.007
NiMo/A-K(3)	0.013	0.000	0.009

Table 5
XPS chemical state of oxide catalysts precursors.

Catalyst	Co $2p_{3/2}$			Ni $2p_{3/2}$		Mo $3d_{5/2}$	
	BE	FWHM	[a]I_p/I_s	BE	FWHM	BE	FWHM
CoMo/A	781.8	3.7	0.76	–	–	232.6	2.2
CoMo/A-K(1)	781.5	3.0	0.80	–	–	232.4	2.0
CoMo/A-K(3)	780.6	3.7	0.83	–	–	232.3	1.6
NiMo/A	–	–	–	856.6	2.6	233.0	2.5
NiMo/A-K(1)	–	–	–	856.3	2.2	232.5	2.0
NiMo/A-K(3)	–	–	–	855.7	2.0	232.5	1.9

[a] Ratio between the intensity of the principal photopeak (I_p) and its satellite (I_s).

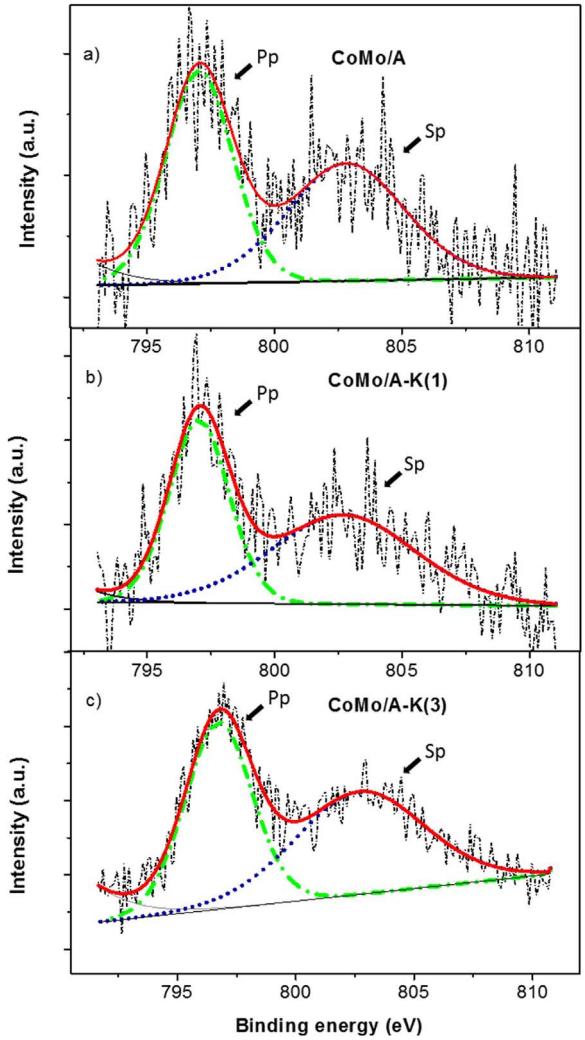

Fig. 5. XPS Co 2p3/2 spectrum for a) CoMo/A, b) CoMo/A-K(1) and c) CoMo/A-K(3) catalysts. Pp = Principal peak, Sp = Satellite peak.

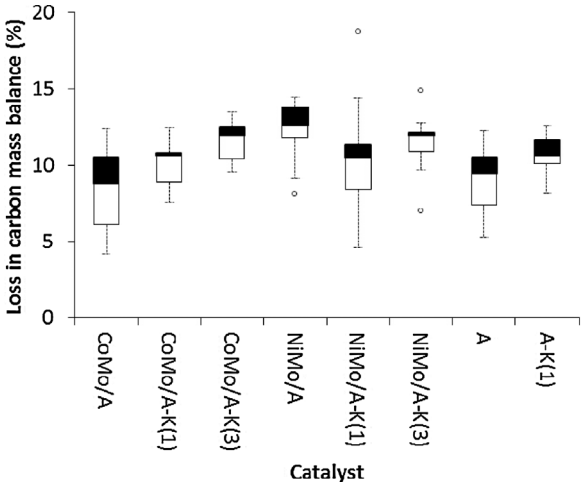

Fig. 6. Percentage loss in carbon mass balance for all catalysts during HDO of guaiacol at 523 K, p_{H2} = 5.5 MPa; catalyst-to-guaiacol ratio of 0.21, and batch reactor.

K(3), increased with its loading, suggesting that the alkali metal disperses very well on the oxide under the present conditions. The incorporation of Mo, Co, and Ni did not seem to affect how potassium is distributed on the surface of alumina since its trend on surface concentration was like the one found for the support. Such a finding is not unexpected since potassium was always impregnated first. It is interesting to analyze the ratios of Mo, Co, and Ni to the elements belonging to the support. To do this, the contribution from carbon adventitious contamination was subtracted from the quantification. The justification for performing such a normalization is twofold: (i) carbon contamination has a very uncertain origin since it can come after adsorption from ambient conditions as well as from X-ray exposure of the samples during the analyses [42]; (ii) although its distribution over the surface is random it seems reasonable to assume that it is merely present as an adlayer at the materials surface. Table 4 features results after applying the announced normalization procedure.

Concerning Mo, the data cannot be interpreted in a straightforward manner. This might well be related to the fact that Mo species deposit on several different surface hydroxyls during preparation [21,30]. In the case of Co and Ni, results indicated an increase in surface Co/(Al + O + K) and surface Ni/(Al + O + K) ratios when increasing potassium loading. Particularly, Table 4 suggests that Co and Ni are better dispersed on CoMo-A-K(3) and NiMo-A-K(3) than on the potassium free materials. This correlates with the formation of surface Co and Ni aluminates discussed from UV–vis DRS results. These aluminates, despite being better distributed on the surface, are considered to be catalytically inactive [43,44].

Besides the changes induced on the surface concentration of the catalytic promoters by potassium, spectra from the Co $2p_{3/2}$, Ni $2p_{3/2}$ and Mo $3d_{5/2}$ core levels of the oxide precursors of the catalysts revealed further evidence on the impact of potassium on the distribution of Mo, Co and Ni surface chemical species. Table 5 lists binding energies (BE) and full widths at half maximum (FWHM) values obtained from the XPS spectra of the Co $2p_{3/2}$, Ni $2p_{3/2}$ and Mo $3d_{5/2}$ core levels of the tested materials.

Concerning Mo, it is notable that the FWHM values of the Mo $3d_{5/2}$ peaks consistently decreased for all potassium loaded materials. This suggests that potassium favors the formation of certain Mo surface species at the expense of others as in agreement to UV-DRS results. Furthermore, the BE of Mo $3d_{5/2}$ shifted to lower values for both CoMo and NiMo based materials. This indicates that potassium promotes the formation of more reduced Mo surface species. Literature [14,30,32] and present UV-DRS results suggest that such a change is a result of the transformation of the polymeric Mo species ($Mo_7O_{24}^{6-}$) into monomeric species (MoO_4^{2-}). Concerning nickel species, Table 5 shows that

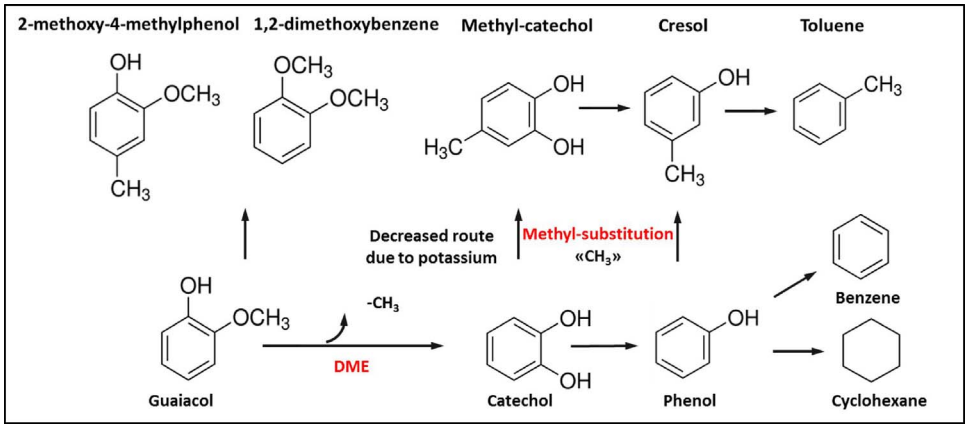

Fig. 7. Reaction scheme for guaiacol HDO (Based on the scheme proposed by Buy *et al*). Reaction conditions: 523 K, p_{H2} = 5.5 MPa; catalyst-to-guaiacol ratio of 0.21.

Table 6
Catalytic activity of the supports and catalysts. Reaction conditions: 523 K, p_{H2} = 5.5 MPa; catalyst-to-guaiacol ratio of 0.21.

Catalyst	k [cm^3/min g]	r_i [molec./min Mo at]
A	0.460	–
A-K(1)	0.050	–
A-K(3)	0.003	–
CoMo/A	0.650	12.2
CoMo/A-K(1)	0.330	7.5
CoMo/A-K(3)	0.170	2.4
NiMo/A	0.720	13.5
NiMo/A-K(1)	0.240	5.7
NiMo/A-K(3)	0.090	2.7

the increment in potassium loading also leads to lower BE values of the Ni $2p_{3/2}$ core level and to a decrease of the FWHM values. Analogous to Mo, such trends can be related to an increase in the relative concentration of surface Ni species in tetrahedral coordination. Considering DRS results, this observation is related to the formation of the $NiAl_2O_4$ spinel phase. Fig. 5 shows the XPS Co $2p_{3/2}$ spectrum and its shake up satellite, located further at 5–6 eV. Analyzing the relative intensity of the Co $2p_{3/2}$ to the satellite peak (I_p/I_s), Table 5, it is observed that the loading of potassium leads to higher values of I_p/I_s. It is known that the satellite peak intensity is very small in the spectrum of Co_3O_4 but very strong in the spectrum of cobalt molybdate [45–47]. Accordingly, the increasing in the I_p/I_s reported in this work (Table 5) can be associated to the formation of Co_3O_4 instead of $CoMoO_4$ species when the catalyst is modified with potassium. The previous analysis is also coherent with the DRS results discussed earlier.

3.2. Influence of potassium on the catalytic performance

The carbon balance was verified for all of the catalysts. In general, the closure in the carbon balance was about 10%–14% except for outliers in these measurements, Fig. 6. Outliers can be ascribed to punctual errors in sample collection during the experiments. Another cause for such outliers might be losses of volatile compounds such as benzene, toluene, cyclohexane or traces of compounds that could not be identified. Notwithstanding, the difference in mass balance, the quantities of compounds quantified are sufficient to determine the performance of the catalysts. Table S7 presents carbon balances in detail.

Fig. 7 exhibits the reaction scheme for guaiacol HDO as based on the products detected herein. The scheme was inspired by the proposal of Bui et al. [7]. Guaiacol conversion can proceed through two main pathways: demethylation (DME) and demethoxylation (DMO). In DME, the hydrogenolysis of the methyl–oxygen bond of the methoxy group ($C_{Aromatic}OCH3$) takes place to form catechol and methane or CH_3^+ species during the first step which is followed by the elimination of one hydroxyl groups from catechol in the second step to produce phenol. In DMO, the methoxy group ($C_{Aromatic}-O-CH_3$) of guaiacol is eliminated

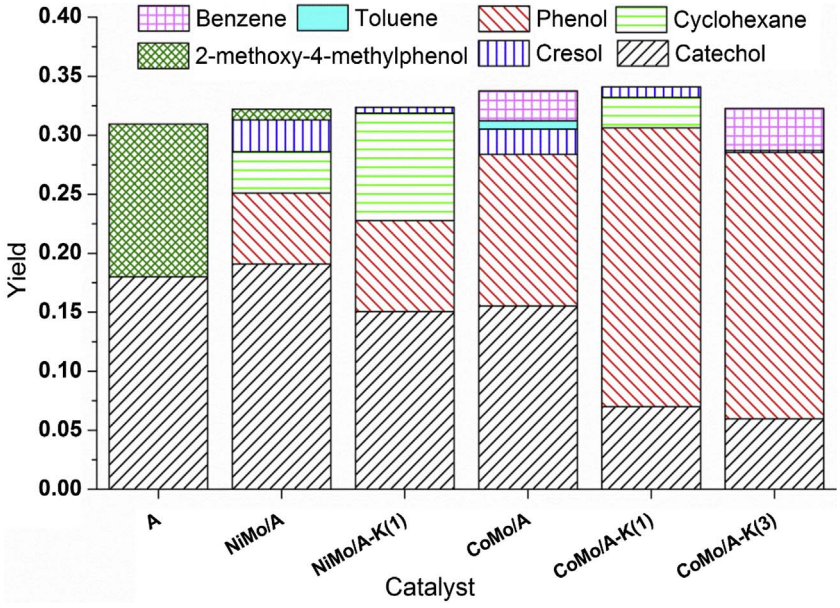

Fig. 8. Products yield at guaiacol iso-conversion (%C = 30%) for alumina and supported CoMo and NiMo catalysts. Reaction conditions: 523 K, p_{H2} = 5.5 MPa; catalyst-to-guaiacol ratio of 0.21.

directly hence producing phenol and methanol. Phenol can actually be further converted via two additional routes: deoxygenation (DDO) to form benzene or a hydrogenation (HYD) mediated removal of the oxygen heteroatom to form deoxygenated products such as cyclohexane [7] plus water. On the other hand, CH_3^+ formed in the DME can act as an alkylating agent for the methylation of catechol or phenol thus leading to formation of heavy methylated products such as methylcatechol and dimethylphenol. The elimination of one of the OH groups of this molecule leads to the formation of cresol.

The reaction rate constant (k) and the apparent reaction rate (r_i) of both the sulfided catalytic supports and the catalysts are reported in Table 6. In addition, Fig. 8 shows the products yields of guaiacol HDO

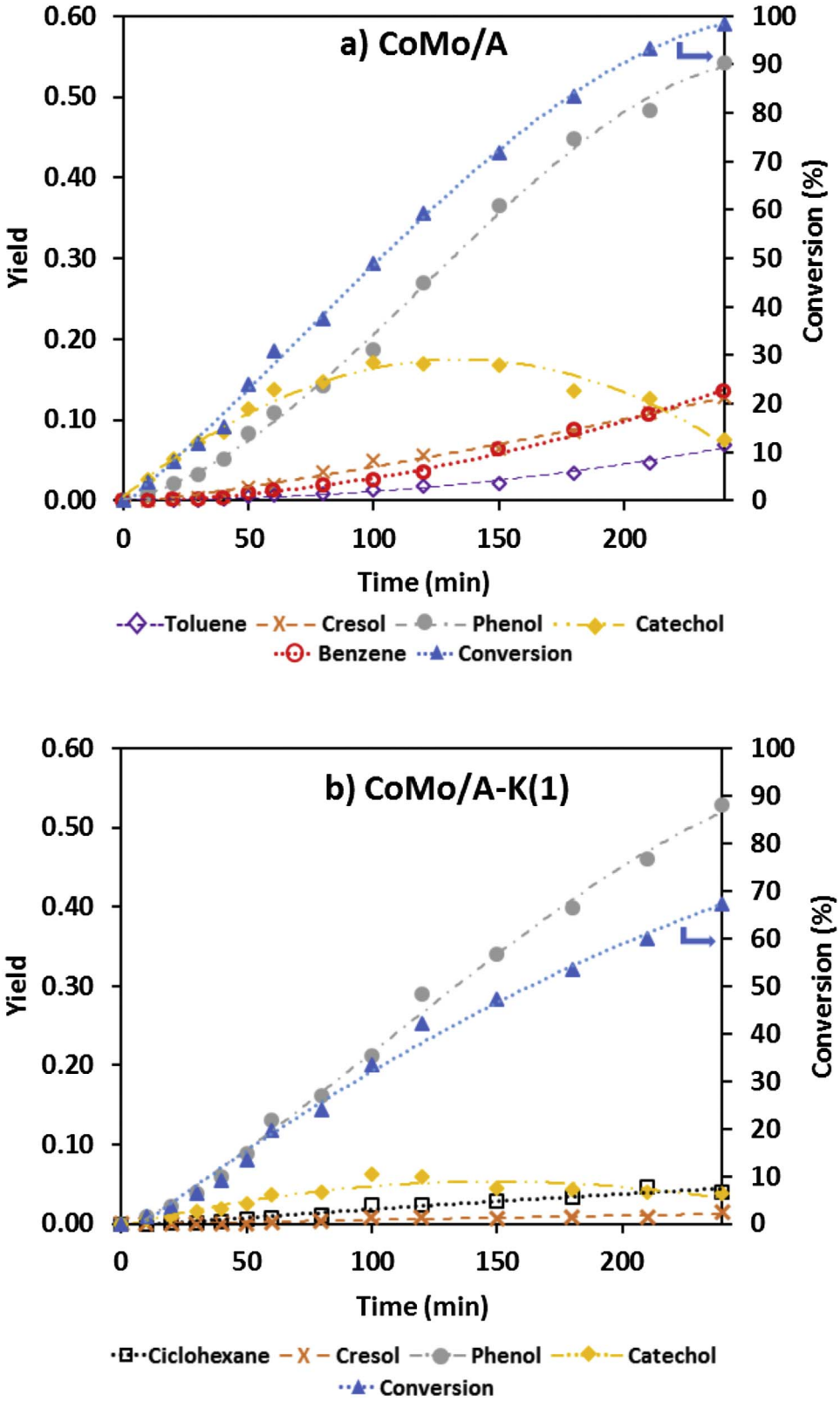

Fig. 9. Curves of products yields and conversion of guaiacol as a function of time for catalysts: a) CoMo/A, b) CoMo/A-K (1), c) NiMo/A, d) NiMo/A-K (1). In the primary and secondary Y axis are the products yields and the guaiacol conversion, respectively. 4-Methylguaiacol = 2-Methoxy-4-methylphenol. Reaction conditions: 523 K, p_{H2} = 5.5 MPa; catalyst-to-guaiacol ratio of 0.21. Numbers in parentheses indicate the factor by which the values of each serie were multiplied.

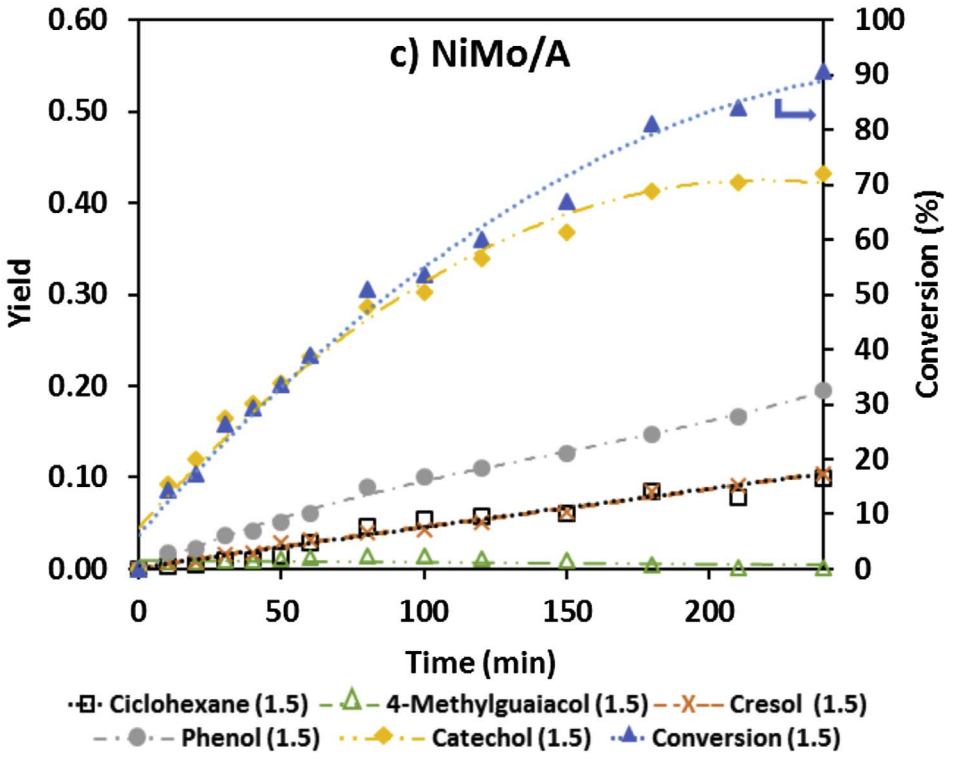

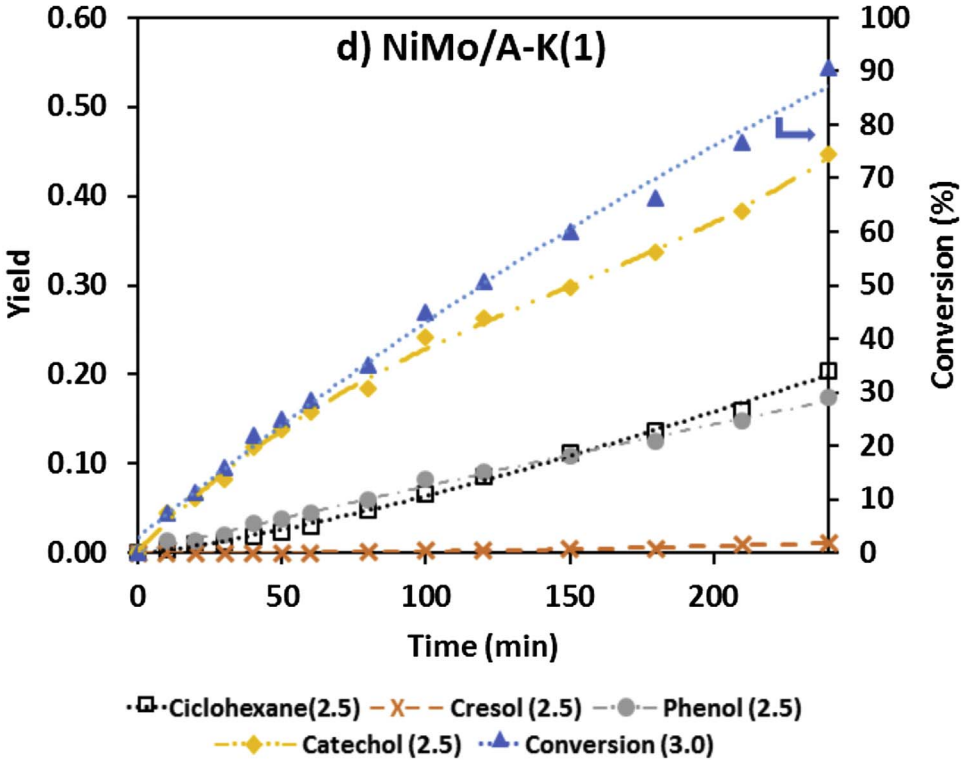

Fig. 9. (*continued*)

at iso-conversion (ca. 30%). According to results, the bare alumina support was active in the reaction and produced catechol, methyl substituted and heavy products. Therefore, alumina promotes the formation of undesired products via the demethylation and the methyl substitution of the aromatic ring of guaiacol. Table 6 also shows that the modification of the alumina with potassium produced a decrease in activity, hence leading to values of the reaction rate constant close to zero for a potassium loading of 3 wt.%. From the activity and selectivity results obtained over alumina, it can be inferred that acid sites act as active sites for the reactions of demethylation and methyl substitution. Bui et al. [7] proposed that the positively charged methyl group yielded by the heterolytic rupture of the methoxy group, which in turn can stay adsorbed on the alumina support instead of being converted to ethane, and subsequently, an electrophilic substitution can occur on the aromatic ring of catechol or phenol. In this research, the results of PAD only allow to indicate that potassium decreases the concentration of OH groups of alumina, but other studies suggest that the alkali metal also tends to adsorb on alumina Al^{3+} sites; which are active sites for methyl-substitution reaction. This could explain the decrease in methylation reactions and thus the activity of the support when it is modified with potassium [27].

CoMo/A and NiMo/A catalysts were more active than alumina and potassium modified alumina. In addition to catechol, these catalysts also produced partially deoxygenated compounds such as phenol, cyclohexane and cresol. Therefore, the sulfided CoMo and NiMo phases promoted both the demethylation of guaiacol and the hydrogenolysis of the aromatic carbon–oxygen bond [7,43]. In this sense, Bredenberg et al. [44] suggested that the hydrogenolysis of the methyl-oxygen bond (DME route) can be carried out both on the surface of the catalytic support and on the surface of the sulfided metallic phases. These findings explain the production of catechol both on alumina as on the sulfided CoMo/A and NiMo/A catalysts.

The modification of the catalysts with potassium generated a positive effect on the selectivity at iso-conversion. Particularly, potassium promoted the production of partially or completely deoxygenated compounds (Fig. 8). For CoMo/A-K(*x*), the addition of potassium promoted phenol promotion and hindered the promotion of catechol and methyl substituted compounds such as cresol and dimethylphenol. For CoMo/A, the concentration of catechol was larger than the concentration of phenol at the start of the reaction (Fig. 9a). Such a trend changed after modifying the support with potassium (Fig. 9b). Indeed, phenol concentration increased at the beginning of the reaction. This may be interpreted as an indication of a direct formation of phenol from guaiacol via the DMO route. Regarding the decrease on the concentration of methyl substituted compounds, a comparison of the reaction products yields of the CoMo/A (Fig. 9a) and NiMo/A (Fig. 9c) catalysts, with their potassium modified counterparts (Fig. 9b and d) shows a decrease in the production of methyl substituted molecules such as cresol and 2-methoxy-4-methylphenol. For NiMo/A-K(x), an increase in the production of cyclohexane was observed followed by a decrease in the yield of methyl substituted compounds (2-methoxy-4-methylphenol and cresol). On the other hand, an increase in the production of phenol and a decrease in the production of cresol was observed for CoMo catalysts. These trends can be ascribed to modifications in acidity induced by potassium hence reflected by the described changes in PAD curves for the oxide precursors of the catalysts. Considering such an effect, one may speculate that there is an increase in the strength of the interaction of guaiacol with the active metallic phase. It must be said that results presented herein are consistent with results reported by other authors in which the alumina is compared with a less acidic support such as activated carbon [9]. Products yields for the other catalysts are presented in Figs. S3, S4, and S5 in the Supplementary Information.

Finally, it must be mentioned that potassium led to a general decrease in the HDO reaction rates (Table 6). These trends agree with characterization results pointing out the promotion of metallic structures which lead to less active sulfided catalysts. To summarize current findings in this regard, potassium promotes the formation of Ni, Co and Mo oxides which are not normally considered suitable precursors of sulfided active sites for HDO. In general, it is conventionally accepted that the active sites for HDO in the catalysts prepared herein are MoS_2 slabs promoted by Co or Ni atoms. Such a conception is based on a model proposed for HDS reactions [43]. Regarding Co and Ni, the present evidence suggests that potassium occupies surface hydroxyls onto which the Ni and Co complexes present in the impregnating metallic solutions normally deposit. In consequence, such metallic complexes might well end up as precursors of less active (or inactive) $CoAl_2O_4$ and $NiAl_2O_4$ spinels.

4. Conclusions

The catalytic hydrodeoxigenation of pyrolysis bio-oils is a step required for producing bio-fuels. However, catalysts normally deactivate quickly due to extensive coke deposition. Herein, potassium was added as a modifier of alumina supported CoMo and NiMo sulfided catalysts. The addition of this alkali metal promoted selectivity to partially and completely deoxygenated compounds in the HDO of guaiacol. Characterization by diverse techniques indicated that potassium changes the acid-base balance of the materials such as to positively influence catalysts selectivity. However, an increase in the relative concentration of Co and Ni aluminate spinels is also promoted. These species are not suitable promoters for sulfided Co-Mo and Ni-Mo active sites thus reducing the catalytic activity.

Acknowledgement

This work was possible due to financial support of the Vicerrectoría de Investigación y Extención de la Universidad Industrial de Santander (VIE-UIS) in the frame of the project with code 1324. Iván D. Mora-Vergara thanks to COLCIENCIAS for his Ph.D. fellowship.

Appendix A. Supplementary data

Supplementary data associated with this article can be found, in the online version, at http://dx.doi.org/10.1016/j.cattod.2017.07.015.

References

[1] D. Mohan, C.U. Pittman, P.H. Steele, Pyrolysis of wood/biomass for bio-oil: a critical review, Energy Fuels 20 (2006) 848–889.
[2] A.V. Bridgwater, Review of fast pyrolysis of biomass and product upgrading, Biomass Bioenergy 38 (2012) 68–94.
[3] P.M. Mortensen, J.D. Grunwaldt, P.A. Jensen, K.G. Knudsen, A.D. Jensen, A review of catalytic upgrading of bio-oil to engine fuels, Appl. Catal. A: Gen. 407 (2011) 1–19.
[4] E.G. Baker, D.C. Elliott, Catalytic upgrading of biomass pyrolysis oils, in: A.V. Bridgwater, J.L. Kuester (Eds.), Research in Thermochemical Biomass Conversion, Springer, Netherlands, 1988, pp. 883–895.
[5] R. Maggi, B. Delmon, A review of catalytic hydrotreating processes for the upgrading of liquids produced by flash pyrolysis, in: B.D.G.F. Froment, P. Grange (Eds.), Studies in Surface Science and Catalysis, Elsevier, 1997, pp. 99–113.
[6] E. Furimsky, Catalytic hydrodeoxygenation, Appl. Catal. A: Gen. 199 (2000) 147–190.
[7] V.N. Bui, D. Laurenti, P. Afanasiev, C. Geantet, Hydrodeoxygenation of guaiacol with CoMo catalysts. Part I: promoting effect of cobalt on HDO selectivity and activity, Appl. Catal. B: Environ. 101 (2011) 239–245.
[8] E. Laurent, B. Delmon, Study of the hydrodeoxygenation of carbonyl, carboxylic and guaiacyl groups over sulfided CoMo/γ-Al_2O_3 and NiMo/γ-Al_2O_3 catalysts: I. Catalytic reaction schemes, Appl. Catal. A: Gen. 109 (1994) 77–96.
[9] A. Centeno, E. Laurent, B. Delmon, Influence of the support of CoMo sulfide catalysts and of the addition of potassium and platinum on the catalytic performances for the hydrodeoxygenation of carbonyl, carboxyl, and guaiacol-type molecules, J. Catal. 154 (1995) 288–298.
[10] C. Sepúlveda, N. Escalona, R. García, D. Laurenti, M. Vrinat, Hydrodeoxygenation and hydrodesulfurization co-processing over ReS_2 supported catalysts, Catal. Today 195 (2012) 101–105.
[11] T. Nimmanwudipong, R.C. Runnebaum, D.E. Block, B.C. Gates, Catalytic conversion of guaiacol catalyzed by platinum supported on alumina: reaction network including hydrodeoxygenation reactions, Energy Fuels 25 (2011) 3417–3427.

[12] G. Busca, Bases and basic materials in industrial and environmental chemistry: a review of commercial processes, Ind. Eng. Chem. Res. 48 (2009) 6486–6511.
[13] T. Montanari, L. Castoldi, L. Lietti, G. Busca, Basic catalysis and catalysis assisted by basicity: FT-IR and TPD characterization of potassium-doped alumina, Appl. Catal. A: Gen. 400 (2011) 61–69.
[14] D.J. Pérez-Martínez, P. Eloy, E.M. Gaigneaux, S.A. Giraldo, A. Centeno, Study of the selectivity in FCC naphtha hydrotreating by modifying the acid–base balance of CoMo/γ-Al_2O_3 catalysts, Appl. Catal. A: Gen. 390 (2010) 59–70.
[15] J. Rouquerol, P. Llewellyn, F. Rouquerol, Is the bet equation applicable to microporous adsorbents? in: F.R.-R.J.R.P.L. Llewellyn, N. Seaton (Eds.), Studies in Surface Science and Catalysis, Elsevier, 2007, pp. 49–56.
[16] E.P. Barrett, L.G. Joyner, P.P. Halenda, The determination of pore volume and area distributions in porous substances. I. Computations from nitrogen isotherms, J. Am. Chem. Soc. 73 (1951) 373–380.
[17] K.S.W. Sing, Reporting physisorption data for gas/solid systems with special reference to the determination of surface area and porosity, Pure Appl. Chem. 57 (1985) 603–619.
[18] L. Vradman, M.V. Landau, D. Kantorovich, Y. Koltypin, A. Gedanken, Evaluation of metal oxide phase assembling mode inside the nanotubular pores of mesostructured silica, Microporous Mesoporous Mater. 79 (2005) 307–318.
[19] J.R. Restrepo-Garcia, V.G. Baldovino-Medrano, S.A. Giraldo, Improving the selectivity in hydrocracking of phenanthrene over mesoporous Al-SBA-15 based Fe–W catalysts by enhancing mesoporosity and acidity, Appl. Catal. A: Gen. 510 (2016) 98–109.
[20] C. Contescu, J. Jagiello, J.A. Schwarz, Proton affinity distributions: a scientific basis for the design and construction of supported metal catalysts, in: J.M.B.D.P.A.J.G. Poncelet, P. Grange (Eds.), Studies in Surface Science and Catalysis, Elsevier, 1995, pp. 237–252.
[21] M. Adachi, C. Contescu, J.A. Schwarz, The use of proton affinity distributions for the characterization of active sites of alumina-supported Co–Mo catalysts, J. Catal. 158 (1996) 411–419.
[22] C. Contescu, J. Jagiello, J.A. Schwarz, Heterogeneity of proton binding sites at the oxide/solution interface, Langmuir 9 (1993) 1754–1765.
[23] E. Laurent, A. Centeno, B. Delmon, Coke formation during the hydrotreating of biomass pyrolysis oils: influence of guaiacol type compounds, in: B. Delmon, G.F. Froment (Eds.), Studies in Surface Science and Catalysis, Elsevier, 1994, pp. 573–578.
[24] B.S. Gevert, J.E. Otterstedt, F.E. Massoth, Kinetics of the HDO of methyl-substituted phenols, Appl. Catal. 31 (1987) 119–131.
[25] V. La Parola, G. Deganello, A.M. Venezia, CoMo catalysts supported on aluminosilicates: synergy between support and sodium effects, Appl. Catal. A: Gen. 260 (2004) 237–247.
[26] H. Knözinger, P. Ratnasamy, Catalytic aluminas: surface models and characterization of surface sites, Catal. Rev. 17 (1978) 31–70.
[27] S. de Miguel, O. Scelza, A. Castro, J. Soria, Characterization of γ-alumina doped with Li and K by infrared studies of CO adsorption and 27Al-NMR, Top. Catal. 1 (1994) 87–94.
[28] S.R. de Miguel, A. Caballero Martinez, A.A. Castro, O.A. Scelza, Effect of lithium addition upon γ-Al2O3 for isopropanol dehydration, J. Chem. Technol. Biot. 65 (1996) 131–136.
[29] H. Pines, W.O. Haag, Alumina: catalyst and support. I. Alumina, its intrinsic acidity and catalytic activity1, J. Am. Chem. Soc. 82 (1960) 2471–2483.
[30] P. Ratnasamy, S. Sivasanker, Structural chemistry of Co-Mo-Alumnina catalysts, Catal. Rev. 22 (1980) 401–429.
[31] J.A. Mendoza-Nieto, I. Puente-Lee, C. Salcedo-Luna, T. Klimova, Effect of titania grafting on behavior of NiMo hydrodesulfurization catalysts supported on different types of silica, Fuel 100 (2012) 100–109.
[32] H. Jeziorowski, H. Knoezinger, Raman and ultraviolet spectroscopic characterization of molybdena on alumina catalysts, J. Phys. Chem. 83 (1979) 1166–1173.
[33] Y.V. Plyuto, I.V. Babich, I.V. Plyuto, A.D. Van Langeveld, J.A. Moulijn, Synthesis and characterization of molybdenum(VI) oxo-species on the surface of fumed alumina and silica, Colloids Surf. A: Physicochem. Eng. Aspects 125 (1997) 225–230.
[34] D. Mey, S. Brunet, C. Canaff, F. Maugé, C. Bouchy, F. Diehl, HDS of a model FCC gasoline over a sulfided CoMo/Al_2O_3 catalyst: effect of the addition of potassium, J. Catal. 227 (2004) 436–447.
[35] C. Papadopoulou, J. Vakros, H.K. Matralis, G.A. Voyiatzis, C. Kordulis, Preparation, characterization, and catalytic activity of CoMo/γ-Al_2O_3 catalysts prepared by equilibrium deposition filtration and conventional impregnation techniques, J. Colloid Interface Sci. 274 (2004) 159–166.
[36] J. Vakros, C. Kordulis, A. Lycourghiotis, Cobalt oxide supported γ-alumina catalyst with very high active surface area prepared by equilibrium deposition filtration, Langmuir 18 (2001) 417–422.
[37] J. Escobar, M.C. Barrera, A.W. Gutiérrez, J.E. Terrazas, Benzothiophene hydrodesulfurization over NiMo/alumina catalysts modified by citric acid. Effect of addition stage of organic modifier, Fuel Process. Technol. 156 (2017) 33–42.
[38] J. Abart, E. Delgado, G. Ertl, H. Jeziorowski, H. Knözinger, N. Thiele, X.Z.H. Wang, E. Taglauer, Surface structure and reduction behaviour of Nio-MoO_3/Al_2O_3- catalysts, Appl. Catal. 2 (1982) 155–176.
[39] P. Atanasova, T. Halachev, Influence of phosphorus concentration on the type and structure of the compounds formed in the oxide form of phosphorus—nickel—molybdenum/alumina catalysts for hydrodesulphurization, Applied Catalysis 48 (1989) 295–306.
[40] R.K.A. Spojakina, S. Damyanova and D. Shopov, in D. Shopov, A., Andreev, A. Palazov and L., P. (Editors), Proc. Vth Int. Symp. Heterog. Catal., Varna, Bulgaria, (1983) 353.
[41] J. Mérida-Robles, E. Rodríguez-Castellón, A. Jiménez-López, Characterization of Ni, Mo and Ni–Mo catalysts supported on alumina-pillared α-zirconium phosphate and reactivity for the thiophene HDS reaction, J. Mol. Catal. A: Chem. 145 (1999) 169–181.
[42] J. Landoulsi, M.J. Genet, S. Fleith, Y. Touré, I. Liascukiene, C. Méthivier, P.G. Rouxhet, Organic adlayer on inorganic materials: XPS analysis selectivity to cope with adventitious contamination, Appl. Surf. Sci. 383 (2016) 71–83.
[43] Y. Romero, F. Richard, S. Brunet, Hydrodeoxygenation of 2-ethylphenol as a model compound of bio-crude over sulfided Mo-based catalysts: promoting effect and reaction mechanism, Appl. Catal. B: Environ. 98 (2010) 213–223.
[44] J.B.s. Bredenberg, M. Huuska, J. Räty, M. Korpio, Hydrogenolysis and hydrocracking of the carbon-oxygen bond: I. Hydrocracking of some simple aromatic O-compounds, J. Catal. 77 (1982) 242–247.
[45] V. La Parola, G. Deganello, C.R. Tewell, A.M. Venezia, Structural characterisation of silica supported CoMo catalysts by UV Raman spectroscopy, XPS and X-ray diffraction techniques, Appl. Catal. A: Gen. 235 (2002) 171–180.
[46] J.E. Herrera, D.E. Resasco, Loss of single-walled carbon nanotubes selectivity by disruption of the Co–Mo interaction in the catalyst, J. Catal. 221 (2004) 354–364.
[47] S.A. Halawy, M.A. Mohamed, G.C. Bond, Characterization of unsupported molybdenum oxide—cobalt oxide catalysts, J. Chem. Technol. Biot. 58 (1993) 237–245.